Homogenization of Mesoscopic Theories: Effective Properties of Model Membranes

R. Lam
Dept. of Chemical Engineering, University of Massachusetts, Amherst, MA 01003

D. G. Vlachos
Dept. of Chemical Engineering and Center for Catalytic Science and Technology (CCST), University of Delaware, Newark, DE 19716

M. A. Katsoulakis
Dept. of Mathematics and Statistics, University of Massachusetts, Amherst, MA 01003

A new mathematical framework for modeling diffusion in nanoporous materials or on surfaces exhibits heterogeneity in properties over large length scales and retains molecular scale information, typically captured only by molecular simulations (kinetic Monte Carlo). It first uses newly developed mesoscopic equations derived rigorously from underlying master equations by coarse-graining statistical mechanics techniques. Homogenization techniques are then used to derive the leading-order effective mesoscopic models that are subsequently solved by spectral methods. These solutions are also compared to direct numerical simulations for selected 2-D model membranes with defects, when attractive adsorbate-adsorbate interactions affect particle diffusion. Both the density and dispersion of defects significantly alter the macroscopic behavior in terms of fluxes and concentration patterns, especially when phase transitions can occur. In the presence of adsorbate-adsorbate interactions, permeation through a nanoporous film can depend on the face of a membrane exposed to the high-pressure side. Homogenization techniques also could offer a promising alternative to direct numerical simulations, when complex, large-scale heterogeneities are present.

Introduction

The introduction of Monte Carlo (MC) techniques (Metropolis et al., 1953) in conjunction with the rapidly increasing computational power have revolutionized our understanding about the mesoscopic structure, thermodynamic, and transport properties of a large spectrum of problems for which molecular interactions are important. Examples include bulk liquids, solids, surface reconstruction phenomena, protein folding, and crystallization (Allen and Tildesley, 1989; Binder, 1986, 1992; Cummings et al., 1997; Thompson, 1999). Aside from equilibrium problems, MC methods, especially on a lattice, have been successfully employed for irreversible problems such as crystal growth, catalytic reactions, and diffusion/reaction in nanoporous materials such as zeolites [see recent review articles and citations therein (Auerbach, 2000; Chuan Kang and Weinberg, 1995; Gilmer, 1980; Gomer, 1990; Keil et al., 2000; Tsikoyiannis and Wei, 1991; Zhdanov and Kasemo, 1994; Ziff et al., 1986)]. These MC simulations are often referred to as kinetic MC (KMC) or continuous time MC (CTMC) methods, and are usually some derivative of the work of Gillespie and Kalos and Lebowitz (Bortz et al., 1975; Gillespie, 1976, 1977). A comparison of time scales between various KMC algorithms, even for algorithms often reported in MC events or steps, is given in Reese et al. (2001). KMC simulations directly solve an underlying master equation, and given sufficient information about transition probabilities, they provide its exact solution. It is this class of molecular models that we refer to in this article and that is typically encountered when the activation energy of hopping is sufficiently larger than the thermal energy (in practice it may not have to be much higher (Auerbach, 2000)). In this case, the

Correspondence concerning this article should be addressed to D. G. Vlachos.

lattice sites correspond to adsorption sites whose distance is in the subnanometer length scale.

Despite the enormous progress achieved so far, KMC simulations are computationally very intensive and limited to relatively small time and length scales. The issue of length scales is not restrictive when only microscopic inhomogeneities are present as a result, for example, of intermolecular forces. These typically can be adequately captured via periodic boundary conditions and sufficiently large simulation boxes. However, there are three broad classes of problems, which are currently intractable by KMC simulations due to macroscopic inhomogeneities. The first class includes systems that exhibit mesoscopic or macroscopic patterns as a result of self-regulation mechanisms. Examples include Turing patterns (Turing, 1952) and patterns resulting from the competition of microphase separation, driven by attractive interactions, and chemical reaction (Hildebrand et al., 1998; Horntrop et al., 2001). The second class encompasses forced systems that operate under an overall macroscopic gradient in one or more variables (such as concentration, temperature, and so on). Examples include transport through membranes, catalytic reactors, and chemical vapor deposition reactors. The last class involves systems that exhibit intrinsic heterogeneity in properties over relatively larger scales than those amenable to KMC simulations. Examples include composite materials, heterogeneous catalysts, and materials with mesoscopic defects. To our knowledge, problems in this last class in which intermolecular forces dictate microscopic mechanisms of transport and chemistry have not been previously addressed and are therefore the focus of this article.

A recently introduced mesoscopic approach (De Masi et al., 1994; Giacomin and Lebowitz, 1998; Hildebrand and Mikhailov, 1996; Vlachos and Katsoulakis, 2000) based on coarse-graining of the underlying master equation provides a promising alternative to KMC simulations when larger scales need to be considered. Such mesoscopic models can describe exactly, that is, at the same level as KMC simulations, the role of intermolecular forces in diffusion under certain conditions. Mesoscopic equations retain the nature of the microscopic dynamics that they are based upon (for example, Metropolis vs. Arrhenius). They can capture anisotropic interactions and stochastic effects (such as nucleation) and can incorporate multiple additional processes such as desorption, reaction, and adsorption. Recent numerical simulations and theoretical results have demonstrated the excellent performance of this novel approach (Katsoulakis and Vlachos, 2002; Lam et al., 2001; Vlachos and Katsoulakis, 2000), as briefly outlined in the next section. As continuum equations, numerical solutions of mesoscopic equations can be easily and efficiently obtained for long time and large length scales, especially when spectral algorithms are employed (Horntrop et al., 2001). Therefore, solutions of the aforementioned first two classes of spatially inhomogeneous systems can be systematically obtained.

We extend here this mathematical mesoscopic framework to the third class of spatially inhomogeneous materials. In particular, an effective mesoscopic diffusion model, including strong interparticle interactions and material heterogeneity, is formulated. This new mathematical framework is applied to model membranes in 2-D. After briefly introducing the features of the mesoscopic equations, homogenization techniques are briefly reviewed and applied. The latter approach enables us to develop approximate solutions for heterogeneous systems in different scaling regimes. Effective permeation properties of model membranes are then computed under an overall concentration gradient using both direct numerical simulations and homogenization. Direct numerical simulations, using spectral methods, allow us to validate the homogenized solutions and to examine the effect of heterogeneity on concentration patterns and on the overall permeation behavior. Finally, conclusions are drawn.

Mesoscopic Modeling

The mesoscopic equations are coarse-grained limits of the master equations as the range of the interaction potential approaches infinity and are exact in this limit. Although mesoscopic equations can be derived for a variety of processes (De Masi et al., 1994; Giacomin and Lebowitz, 1998; Hildebrand and Mikhailov, 1996; Vlachos and Katsoulakis, 2000), we mainly focus on diffusion. For Metropolis and Arrhenius microscopic dynamics, the respective mesoscopic diffusion equations under isothermal conditions are (Vlachos and Katsoulakis, 2000)

$$\frac{\partial u}{\partial t} = d\nabla\cdot\left[\nabla u - \beta u(1-u)\nabla K^* u\right] \tag{1}$$

$$\frac{\partial u}{\partial t} = D\nabla\cdot\left\{e^{-\beta K^* u}\left[\nabla u - \beta u(1-u)\nabla K^* u\right]\right\} \tag{2}$$

where u is the coverage (dimensionless concentration), $D = de^{-\beta U_o}$ is the diffusion coefficient, d is the diffusion coefficient at high (infinite) temperature, U_o is the energy associated with the binding to the host, K is the intermolecular potential of adsorbate-adsorbate interactions, $K^*u = \int K(|r-r'|)u(r')dr'$ is the convolution, and $\beta^{-1} = kT$, with k being the Boltzmann constant and T being the temperature. Additional microscopic dynamics can also be considered, but is beyond the scope of this article.

Regarding the physical significance of these equations, the lefthand side of Eqs. 1 and 2 describes the accumulation term, whereas the first term on the righthand side represents the normal Fickian diffusion (Laplacian term) that occurs in the absence of interactions. The term $u(1-u)$ represents that the probability of migration depends on having a site occupied multiplied by the probability that a neighboring site is empty (note that, in the continuum, representation of the indices of lattice sites has dropped out). Finally, the convolution term represents the energy that a species at position x feels from its neighbors due to adsorbate-adsorbate interactions. Thus, the entire second term on the righthand side represents the modification of the diffusion process due to interactions.

Equations 1 and 2 can also be written in a more conventional way where the flux is expressed in terms of the chemical potential gradient. As an example, for Arrhenius dynamics, by introducing the free energy $E[u] = -\int\int K(r-r')u(r)u(r')drdr'/2 + \beta^{-1}\int[u\ln u + (1-u)\ln(1-u)]dr$, the flux can be written as $j = -\mu[u]\nabla[(\delta E[u])/\delta u]$, where the mobility is $\mu[u] = D\beta u(1-u)\exp(-\beta K^* u)$ (Vlachos and Katsoulakis, 2000). Note that the mobility is nonconstant. Furthermore, it can be shown that Eqs. 1 and 2 can be re-

duced, under certain assumptions (Horntrop et al., 2001; Katsoulakis and Vlachos, 2002) to the classic Cahn-Hilliard equation of spinodal decomposition.

We should remark that Eqs. 1 and 2 consider a fundamental diffusivity that is concentration-independent. However, the presence of interactions in Eqs. 1 and 2 gives rise to a concentration-dependent effective diffusion coefficient, if the constitutive equation of the flux is written as proportional to the concentration or loading gradient. This issue and the possibility of simply using a modification of Fick's first law (with variable diffusivity) in accounting for interactions is analyzed in Lam et al. (2001), where the factors affecting the concentration-dependence of the effective diffusivity are also presented.

For many systems, the range of the interactions can typically be relatively short suggesting that mesoscopic models may have limited accuracy. However, it has been previously shown, via 1- and 2-D simulations (Lam et al., 2001; Vlachos and Katsoulakis, 2000), that the mesoscopic formalism can still yield accurate results even for relatively short-range interactions because these equations exhibit a large deviation principle (Katsoulakis and Vlachos, 2002). The latter principle suggests that the infinite potential length case results should be approached exponentially fast as the potential length increases. These conclusions appear independent of details of the potential (attractive or repulsive, piecewise constant or continuous, and so on) and microscopic mechanisms of diffusion. In fact, as often happens with the global mean field theory for equilibrium problems, theoretical predictions and numerical simulations suggest that excellent agreement is attained with shorter potentials in higher dimensions or larger coordination lattices.

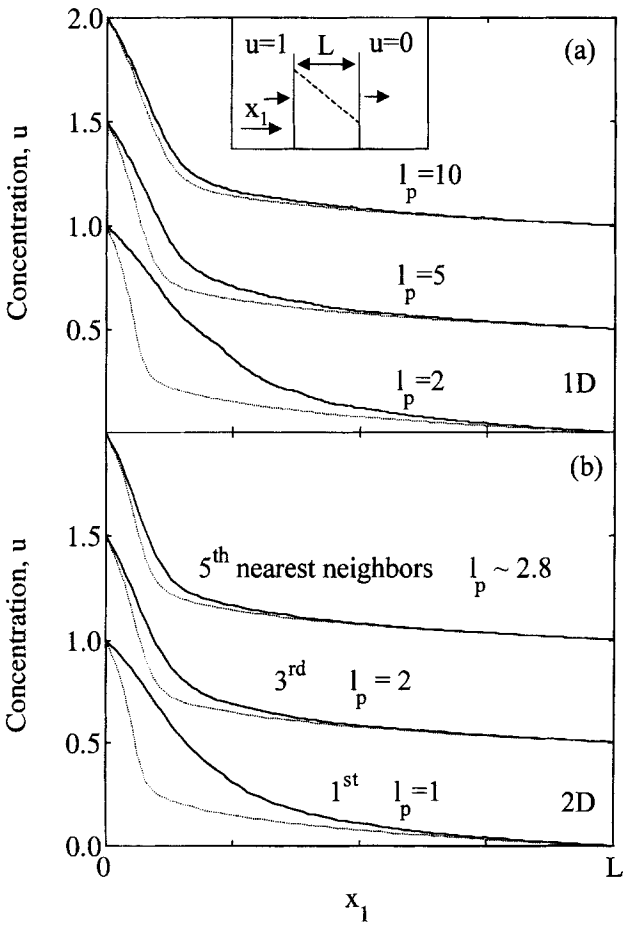

Figure 1. Comparison of 1-D and 2-D concentration from gradient continuous time MC (—) and mesoscopic simulations (----) for various lengths of the intermolecular potential.

The inset in panel (a) depicts the geometry studied in 1-D along with the boundary conditions. The potential in these simulations is $\beta K N_p = 4$ up to a distance of l_p and zero otherwise.

As an example, Figure 1 compares results from 1- and 2-D gradient continuous time MC (G-CTMC) simulations (solid lines) (Lam et al., 2001; Vlachos and Katsoulakis, 2000) to those from the corresponding mesoscopic equation (dashed lines) for diffusion under an overall concentration gradient, for the geometry depicted in the inset of Figure 1a. Dirichlet boundary conditions of 1 and 0 in the concentration are imposed in the direction of transport, and periodic boundary conditions are imposed in the transverse one in the 2-D simulations. A piecewise constant potential of constant strength (attractive interactions) was used in these simulations. In particular, the potential was taken constant and equal to $K = w/Np$, where N_p is the number of neighbors within the range of the potential l_p, and zero otherwise. Arrhenius microscopic dynamics (Vlachos and Katsoulakis, 2000) was employed in these simulations. The upper two concentration profiles in each panel are shifted on the vertical axis for clarity.

Excellent agreement between the two approaches (KMC and mesoscopic) is achieved even for relatively short-range interactions. Despite some deviations seen in concentration profiles for short potentials (such as $l_p = 1$), the corresponding fluxes of the G-CTMC and mesoscopic models differ only up to a few percent (Lam et al., 2001). Furthermore, comparable deviations between the 1- and 2-D simulations are observed for potential lengths in 2-D roughly equal to the square root of those in 1-D. This dimensionality effect has rigorously been shown theoretically in Katsoulakis and Vlachos, (2002), and indicates that shorter potentials are needed in higher dimensions to reach the infinite range scale results.

In the next section, effective mesoscopic diffusion equations for heterogeneous systems will be derived using homogenization techniques. While the results are independent of boundary conditions, in later sections, the configuration depicted in the inset of Figure 1a will be used as a prototype example to compute effective properties. This configuration physically mimics permeation experiments through nanoporous films, such as those encountered in zeolite membranes. An example of the microstructure of an MFI zeolite supported film fabricated by the secondary growth technique, which was obtained recently using laser confocal microscopy (Bonilla et al., 2001), is shown in Figures 2f and 2g. The bright areas indicate grain boundaries (defects) within the zeolite film. More defects are observed near the alumina substrate at the bottom of the film. As shown below, this asymmetry in microstructure is important regarding permeation properties, when intermolecular forces are important. We do not attempt to model realistic systems mainly because the meso-

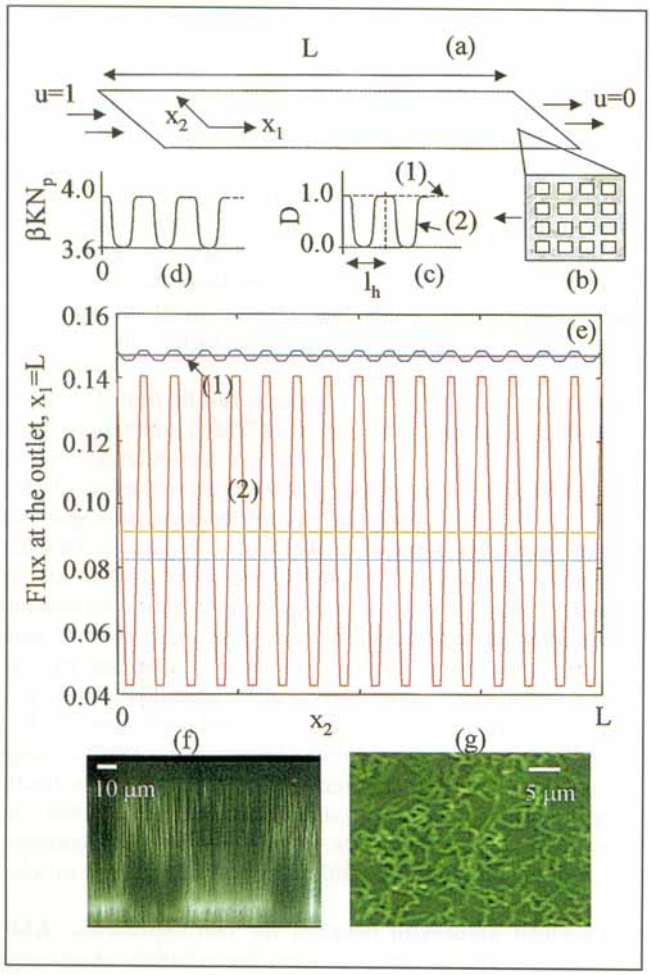

Figure 2. Scales and validation of the homogenized equations.

System configuration and the macroscale x (a); magnification of heterogeneous medium with normal material (shaded) and defects (white squares), (b) diffusion coefficient (c) and interparticle potential (d) plotted in 1-D, and fluxes at the outlet (e), from the homogenized equation (horizontal dashed lines) and direct numerical simulations (solid, oscillating lines). Typical microstructure obtained from fluorescence laser confocal microscopy of a supported MFI zeolite membrane in cross section (f) and top view of the surface (g) (Bonilla et al., 2001). The solid horizontal lines are spatially averaged fluxes from direct numerical simulations. For these simulations, the heterogeneity in case (1) is in the potential ($N_p\beta w_{\text{defect}} = 3.6$, $N_p\beta w_{\text{material}} = 4$) and in case (2) in both the potential ($N_p\beta w_{\text{defect}} = 3.6$, $N_p\beta w_{\text{material}} = 4$) and the diffusion coefficient ($D_{\text{defect}} \sim 0$, $D_{\text{material}} = 1$). The parameters are $l_p = 30$ and $l_h = 4$. The homogenized equations are in good agreement with direct numerical simulations.

scopic equations, in their current form, are not suitable to describe the complex lattice of zeolites.

Homogenization

Homogenization techniques are a set of formal mathematical procedures that allow for the inclusion of smaller-scale heterogeneities in a larger-scale problem. The mathematical foundations can be found in Bensoussan et al. (1978), Sanchez-Palencia (1980) and Sanchez-Palencia and Zaoui (1986) and have been applied to a large variety of problems, including composite materials modeling (Cruz and Patera, 1995), porous media (Auriault and Ene, 1994; Bouddour et al., 1998; Cioranescu and Saint Jean Paulin, 1998; Mei et al., 1996), and climatic and geomechanic modeling (Murad, 1999). Their major advantage is that they can provide effective properties of a relatively large heterogeneous medium for which application of direct numerical simulations is too intensive.

In the problem of interest, there are several scales present, as shown in Figure 2. These include the microscopic lattice constant (site-to site-jump distance), the interaction potential scale l_p (panel c), the heterogeneity scale l_h which represents the length scale statistically capturing the variations in the materials properties (panel b) (that is, a statistically representative ensemble of crystallites and grain boundaries in the case of polycrystalline zeolite films), and the macroscopic system scale L (panel a), making the problem intrinsically multiscale. The heterogeneity scale is taken to be much smaller than the macroscale, which is equivalent here to assuming that the heterogeneity is periodic, although it is possible to apply homogenization to randomly distributed systems (Poutet et al., 1996). In the numerical examples considered below, the macroscopic and heterogeneity scales have the units of the cutoff distance of the potential.

With the assumption $l_h \ll \mathrm{L}$, three different scaling regimes can still appear. The potential range (cutoff distance) can be smaller than, similar to, or larger than the heterogeneity scale. Although the methodology is very general, for clarity, the homogenization procedures will be presented here for one scaling regime only, the case when the potential range is much larger than the heterogeneity scale. This situation may arise when long-range electrostatic interactions dominate. Let us define a macroscopic variable x, $x = (x_1, x_2)$ in 2-D that describes the behavior at the scale L and similarly a microscopic variable y that describes the behavior at the small scale l_h, as depicted in Figure 2, so that the following relations hold

$$\epsilon = \frac{l_h}{L} \ll 1 \text{ and } y = \frac{x}{\epsilon}$$

The heterogeneity of the material can manifest itself in the diffusion coefficient and/or in the interparticle interactions. Let $D = D(y)$ be periodic in the microscale y (l_h periodic) and $K = K(x,y)$. For spherical symmetric potentials, the interaction physically between two particles depends only on the distance between them and the nature of the medium around each particle. The distance between two particles can be greater or smaller than the characteristic length associated with the heterogeneity scale. Therefore, K depends on both x and y. The nature of the medium at the position of the particle is purely dependent on the microscale, since the heterogeneity is taken to be microscopic. Thus, we will consider a potential of the form

$$K(x_A, x_B, y_A, y_B) = J(|x_A - x_B|)a(y_A)b(y_B) \qquad (3)$$

Here, J corresponds to the "distance" term and would represent the interaction potential in a homogeneous medium; a and b are the "medium indicator" terms. For simplicity in

the homogenization procedure, the terms a and b are taken to be symmetric ($a = b$) and their variation in amplitude is taken to be of the same order as the characteristic scale of the heterogeneity. This symmetry arises physically from the fact that a pair of particles A and B interacts the same way, whether viewed from A or B. In the more general case, where the amplitude of the variations in the potential caused by heterogeneities is unrelated to the size of the heterogeneity, another small parameter could be introduced to characterize the variations of the potential. This would render the homogenization procedure a multiple parameter expansion. The terms a and b are taken to be weakly convergent, here, so that they can be expressed as

$$a = a_0 + \epsilon a_1 + \epsilon^2 a_2 + \cdots \tag{4}$$

$$b = b_0 + \epsilon b_1 + \epsilon^2 b_2 + \cdots \tag{5}$$

The concentration in the mesoscopic equation depends on both scales and is expanded as

$$u = u(x, y, t) = u_0 + \epsilon u_1 + \epsilon^2 u_2 + \cdots \tag{6}$$

Using the above notation, as an example in the Metropolis case, we can recast Eq. 1 as follows

$$\frac{\partial u}{\partial t} = \nabla\cdot\left[D(y)\left[\nabla u(x,y) - \beta u(x,y)(1-u(x,y)) \times \nabla\left(\int J(|x-x'|)a\left(\frac{x}{\epsilon}\right)b\left(\frac{x}{\epsilon}\right)u\left(x',\frac{x'}{\epsilon}\right)dx'\right)\right]\right] \tag{7}$$

The first step in obtaining the homogenized effective equation is expanding Eq. 7 using Eq. 6, Eq. 5, and Eq. 4 to form cell boundary-value problems at each order of ϵ. The leading order problem is homogeneous and its solution is either independent of the microscopic scale or indeterminate. Next, linearity is invoked to express the higher-order solutions in terms of the leading-order one and construct an inhomogeneous canonical cell problem. From this inhomogeneous cell problem, the effective governing equation of the leading order can be expressed. In this example, the inhomogeneous cell problem is reached at the second order of ϵ. The full derivation of the homogenized equation, for Metropolis and Arrhenius microscopic dynamics and possible reaction terms, can be found in Lam (2001). Here, the homogenized equation (leading order solution) for the purely diffusive cases is

$$\frac{\partial u_0}{\partial t} = \sum_k \frac{\partial}{\partial x_k}\left[\sum_i D_{ki}^{\text{eff}} u_0(1-u_0)\frac{\partial}{\partial x_i}\left(\ln\left[\frac{u_0}{(1-u_0)}\right] - \beta a_0 b_0 J * u_0\right)\right] \tag{8}$$

with

$$a_0 = \frac{1}{\Omega}\int_Y a(y)dy \tag{9}$$

$$b_0 = \frac{1}{\Omega}\int_Y b(y)dy \tag{10}$$

$$\Omega = \int_Y dy \tag{11}$$

$$D_{ki}^{\text{eff}} = \frac{1}{\Omega}\int_Y\left[D\left(\delta_{ik} + \frac{\partial \chi_i}{\partial y_k}\right)\right]dy$$

for Metropolis dynamics (12)

$$D_{ki}^{\text{eff}} = \frac{1}{\Omega}e^{-a_0 b_0 K * u_0}\int_Y\left[D\left(\delta_{ik} + \frac{\partial \chi_i}{\partial y_k}\right)\right]dy$$

for Arrhenius dynamics. (13)

Here, δ is the Kronecker symbol and χ is the solution of

$$\sum_k\sum_l\left[\frac{\partial}{\partial y_l}\left(D\frac{\partial \chi_i}{\partial y_k}\right)\right] = -\sum_l \frac{\partial D}{\partial y_l} \tag{14}$$

over the heterogeneity scale l_h. All the summations extend over the dimensionality of the problem.

Solution of the homogenized Eq. 8 for the leading-order solution u_0 requires the effective diffusivity D_{ki}^{eff} that depends on the heterogeneity of the materials, that is, the variation of diffusivity with space and the geometry (spatial distribution of defects). The effective diffusivity can be obtained for a periodic domain Y using either Eq. 12 or 13, depending on the microscopic dynamics. In turn, χ needed in Eq. 13 or 14 is obtained from solving Eq. 14 which is reminiscent of a diffusion-reaction equation. Numerical techniques to carry all these out are described below.

We close this section with a brief discussion on the other scaling regimes. When the potential range is of the same order as the scale of the heterogeneity, only the definition of the potential K differs from the above case and becomes

$$K(y_A, y_B) = Z(|y_A - y_B|)a(y_A)b(y_B) \tag{15}$$

Both the distance term and the medium indicator term in the interaction potential depend here only on the microscale. Because of the scaling within the distance term, the potential Z is of the form

$$Z = \epsilon^{-n}J\left(\frac{x_A}{\epsilon} - \frac{x_B}{\epsilon}\right) = \epsilon^{-n}J(y_A - y_B) \tag{16}$$

where n is the dimensionality of the problem. This scaling arises succinctly, from the fact that the macroscale system should perceive the contribution of particles only in a small region of the domain of the order of the potential range. The derivation of the effective mesoscopic equation in this case is not shown, but is analogous to the previous case with the exception that the inhomogeneous cell problem is reached for terms of fourth order in ϵ, so the algebra becomes more complicated. Finally, for the remaining case, where the interaction range is much smaller than the heterogeneity, a sec-

ond microscale variable must be introduced

$$\eta = \frac{l_p}{l_h} \gg 1 \quad \text{and} \quad s = \frac{y}{\eta} \tag{17}$$

For example, if $\eta = \epsilon^m$, the distance term in the interaction potential could be written as

$$Z = \epsilon^{-nm} J\left(\frac{y_A}{\epsilon^m} - \frac{y_B}{\epsilon^m}\right) = \epsilon^{-nm} J(s_A - s_B) \tag{18}$$

In the following sections, an overview of the numerical techniques used is given, followed by the presentation of the numerical validation of the effective mesoscopic equation for the first scaling regime. Finally, direct numerical results for various scaling regimes are presented to elucidate the role of heterogeneity in concentration patterns and effective permeation properties.

Numerical Techniques

The mesoscopic equations presented are solved in 2-D using spectral methods along with a Newton-Krylov solver (Kelley, 1995). The boundary conditions are chosen so that an overall gradient is present in the x_1 direction, where a Chebyshev polynomials based approach is used. In the perpendicular x_2 direction, periodic boundary conditions are used, and a fast Fourier transform (FFT) based approach is employed. The use of Chebyshev polynomials as interpolant requires an unequally spaced discretization defined by the Chebyshev points (Trefethen, 2000)

$$x_{\text{cheb}}(k) = \cos\left(\frac{\pi k}{n}\right) \quad \text{with} \quad k = 1, \ldots, n. \tag{21}$$

Although Unequally-Spaced Fourier transform (USFFT) procedures do exist (Beylkin, 1995; Press et al., 1986), for simplicity, the convolution products in the mesoscopic equations are computed here on an interpolated uniform grid, along with virtual induced periodicity (Lam et al., 2001) in the direction of the gradient so that regular FFT can finally be used. The virtually periodic extended domain also accommodates the boundary conditions, as shown in Figure 3.

For simplicity, a piecewise constant interaction potential J, used also in Figure 1, is employed

$$J(|r - r'|) = \frac{w}{N_p} \qquad \text{if } |r - r'| \le l_p,$$

$$J(|r - r'|) = 0 \qquad \text{if } |r - r'| > l_p,$$

where w is the interaction strength, l_p is the interaction range, and N_p is the number of neighbors within the radius of the cutoff distance of the potential.

For the solution of the homogenized problem, given the possible variations of the diffusivity, an FFT approach with fully periodic boundary conditions is used to solve Eq. 14. Its solution permits the complete evaluation of the integrals in Eqs. 12 and 13 by an adaptive recursive Simpson's rule scheme

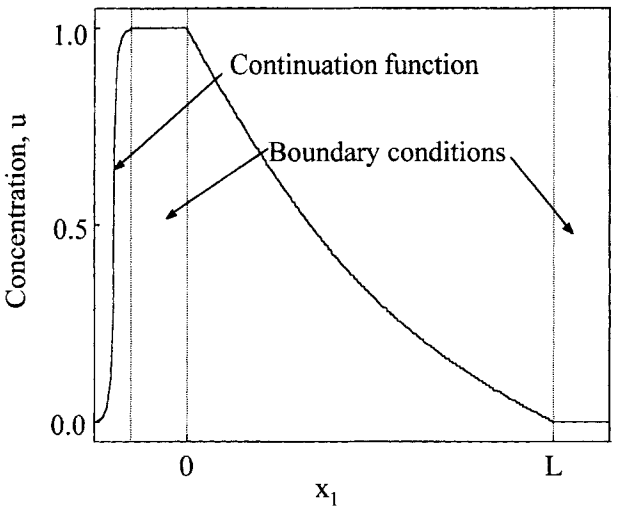

Figure 3. Induced virtual periodicity for application of FFT in the direction of transport.

(done in Matlab). The effective diffusion coefficients given by Eqs. 12 and 13 can subsequently be used in Eq. 8. Being of the same form as the original mesoscopic equations, the homogenized Eq. 8 is solved using the spectral techniques described above.

The heterogeneity in properties is introduced numerically using arctangent functions for smoothness and mathematical continuity at interfaces between different materials. An example of variable properties across the period of heterogeneity is depicted in Figures 2c and 2d. For simplicity, we focus on two materials and use the terminology of material and defects to indicate variation between two sets of properties. The whole procedure has been implemented in Matlab. For most simulations, 64x64 nodes are used.

Numerical Results

We first assess the accuracy of the homogenized, effective mesoscopic equations derived. Then, the effect of materials heterogeneity on concentration patterns and flux are examined for a simple configuration before studying the effect of defect dispersion.

Validation of the homogenized equations

To numerically assess the accuracy of the effective mesoscopic equation when the potential range is much larger than the heterogeneity scale, direct numerical simulations are performed for a system satisfying all the relevant assumptions. The simulated model system is depicted in Figure 2a, whereas Figure 2b shows a blowup where white areas correspond to defects (such as grain boundaries) and the shaded ones to the material (such as crystallites of zeolite films). The diffusivity and potential of interactions across the period of heterogeneity are also depicted in Figures 2c and 2d, respectively.

The fluxes obtained from the effective mesoscopic equations and direct numerical simulations as a function of spatial location (in the direction perpendicular to the transport gradient) are shown in Figure 2e for two cases. In case (1), het-

erogeneity is considered in the interaction potential only, and the diffusion is constant (dashed line in Figure 2c). In case (2), the diffusion coefficient varies as well, as shown in Figure 2c. The dashed, horizontal lines depict the results from the homogenized equation, whereas the oscillatory profiles indicate the spatially varying flux at the outlet as obtained from direct numerical simulations. The corresponding spatially average fluxes of direct numerical simulations are shown as horizontal solid lines.

In both cases, the results compare well between the two approaches within the accuracy expected. Indeed, the effective mesoscopic equations are only the leading order equations to which correction terms (of order ϵ or higher) can be added. The substantial spatial variation of flux in case 2 is a result of the strong variation in diffusivities between the normal material and the defects. Note that due to the homogenization procedure, the spatial information in both concentrations and fluxes generally cannot be reconstructed from the solution of the homogenized equation. However, if one is interested in average properties of the entire system, such as permeability, the homogenized equations suffice.

Effect of heterogeneity on concentration patterns and flux profiles

To elucidate the effect of heterogeneity on the system's behavior, we start with a simple heterogeneous configuration of two stripes (material and defect) running along the concentration gradient, as shown in Figure 4a. Several variations in the diffusivity and interaction potential are introduced, including the limiting cases of simple Fickian diffusion (case 1) and pure material with interparticle interactions and no defects (case 2). In the other cases, the interaction potential is taken to be piecewise constant and attractive in the normal material, whereas particles do not interact in the defect. The material adjacent to the inlet and outlet, where concentrations of $u = 1$ and $u = 0$ are imposed, is taken to be of the same nature as the normal one. Microscopic Arrhenius dynamics is considered.

Figures 4b and 4c show the iso-concentration contours and streamlines for case 3 where the diffusivities in the material and defect are equal. Overall, Fickian behavior within the defected domain, and Arrhenius-type behavior, in the normal material, are observed. The streamlines in panel c show that considerable mixing occurs in the direction normal to the imposed gradient. Furthermore, substantial uphill diffusion happens due to attractive interparticle interactions within the normal material. The variation in the diffusivity within the defect (cases 4 and 5) significantly alters the mixing patterns and the flux at the outlet, as shown in Figure 4d. These results indicate that coupling between the material and the defect results in effective properties that are not merely geometrically weighted means of individual elements of the system.

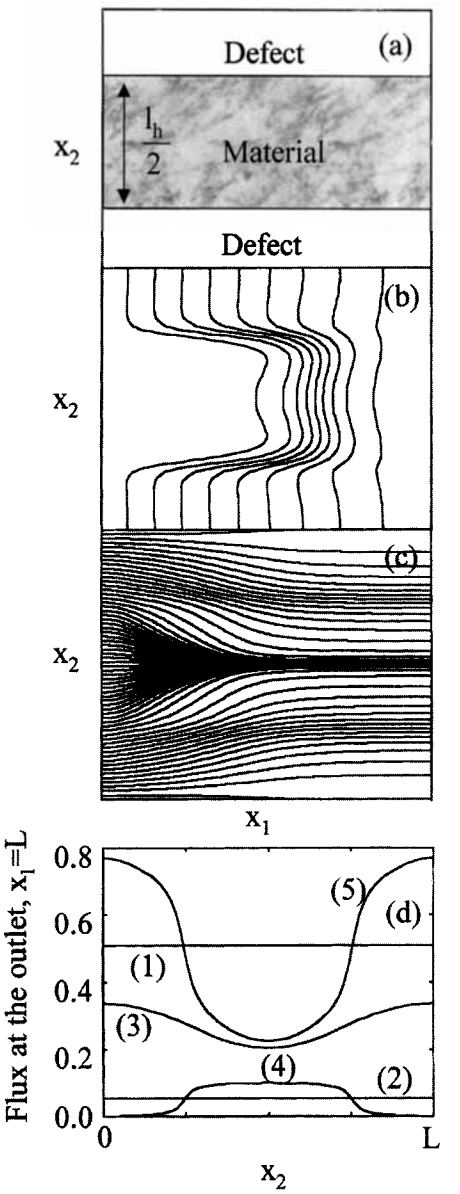

Figure 4. (a) Configuration studied; (b) isoconcentration contours for case 3; (c) streamlines for case 3; and (d) fluxes at the outlet for different cases.

Case 1, $D_{\text{defect}} = D_{\text{material}} = 1$ and no interactions (only normal material with Fickian diffusion); case 2, $D_{\text{defect}} = D_{\text{material}} = 1$ and same interparticle interactions everywhere (only normal material). In cases 3–5, interactions of strength $N_p \beta w = 4$ occur only in the material. Case 3, $D_{\text{defect}} = D_{\text{material}} = 1$; case 4, $D_{\text{defect}} \sim 0$, $D_{\text{material}} = 1$, case 5, $D_{\text{defect}} = 2$, $D_{\text{material}} = 1$. The parameters are $l_p = 5$ and $l_h = 64$. Uphill diffusion in the transverse direction is made apparent when defects are present.

Effect of defect dispersion and membrane asymmetry

To examine the influence of the dispersion of the heterogeneity on the concentration patterns and on the flux at the outlet, direct numerical simulations for different sizes of defects, with defects occupying a constant percentage (25%) of the total area, were performed. In the square-shaped defects, no interparticle interactions occur and the diffusivity is low, whereas in the normal material, particles attract each other according to a piecewise constant potential and diffuse with a constant diffusivity. Both Arrhenius and Metropolis microscopic dynamics were examined. The range of the interaction potential was varied as well in order to examine how solutions vary at different scaling regimes.

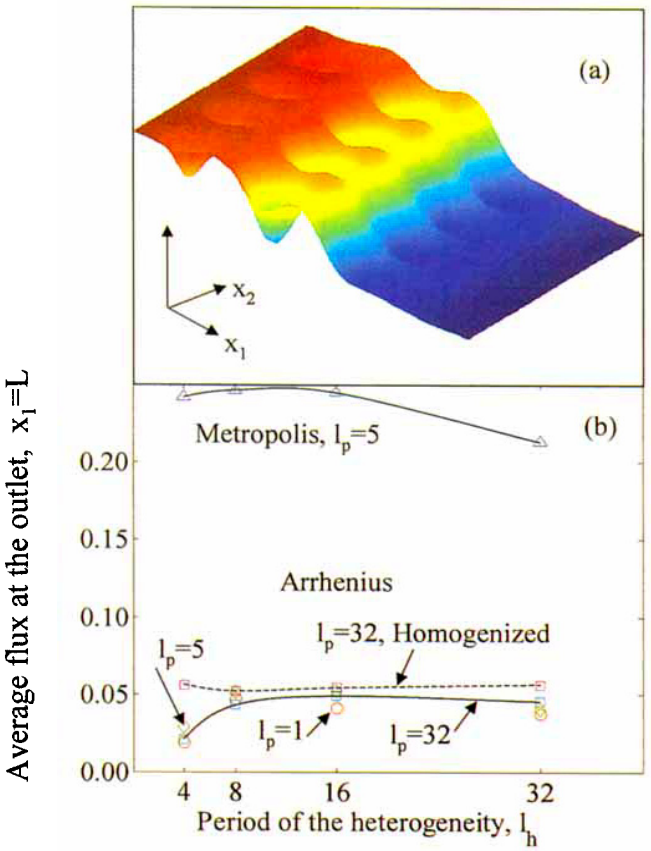

Figure 5. Concentration pattern for $l_p = 5$ and heterogeneities of period $l_h = 16$ using Metropolis dynamics (a) and average fluxes at the outlet vs. period of the heterogeneity (b).

The parameters are $N_p \beta w = 4$, $D_{\text{defect}} \sim 0$, and $D_{\text{material}} = 1$. The homogenized equations were also solved for $l_p = 32$ (dashed line), although the assumption of weak convergence is not justified for the parameter chosen here.

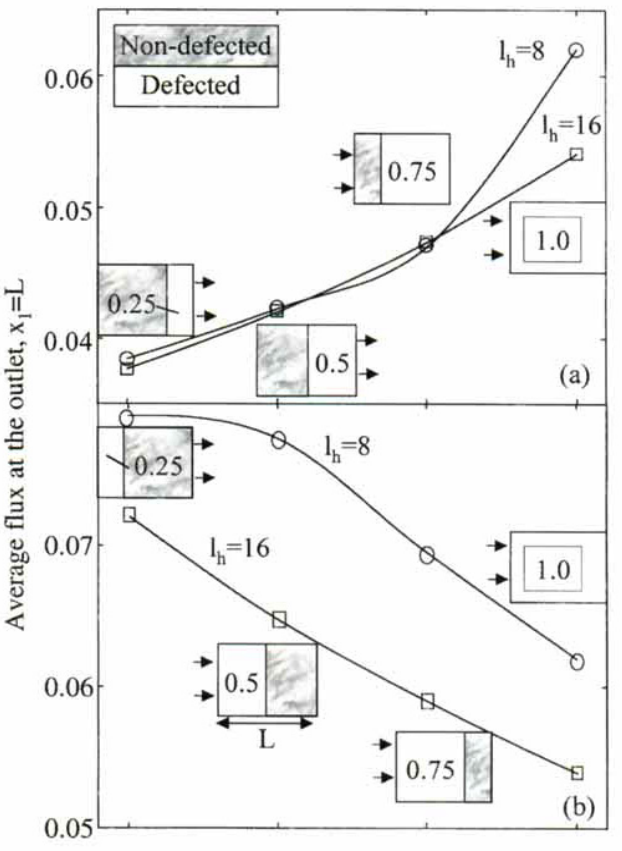

Figure 6. Effect of defect position for two different sizes of heterogeneity ($l_h = 8$ and $l_h = 16$) and for various fractions of defects.

Defects placed near the low-pressure side (a) and defects placed near the high-pressure side (b). The parameters are $D_{\text{defect}} \sim 0$, $D_{\text{material}} = 1$, and $N_p \beta w = 4$.

Figure 5a shows a typical concentration pattern for $l_p = 5$ and $l_h = 16$ using Metropolis dynamics. Here again, considerable 2-D mixing in the transverse direction of the gradient is observed. The overall flux at the outlet as a function of the period of the heterogeneity is depicted in Figure 5b for Arrhenius and Metropolis dynamics and different potential length scales. The results indicate that, even for a given density of defects, their distribution can change the outlet flux by as much as twofold, especially in the Arrhenius case where larger gradients in concentration occur near the entrance of the membrane. This microstructure effect rationalizes one plausible mechanism responsible for the variation of permeabilities of different membranes. It can also be observed in Figure 5b that the dependence of the permeability on the dispersion of defects is nonmonotonic due to concentration patterns and 2-D mixing. Although the parameters chosen here do not comply with the weak convergence assumption for the applicability of the homogenized equations, panel b shows that, for $l_p = 32$, mesoscopic equations still give a reasonable estimate, when the heterogeneity scale to macroscale ratio is of the same order as the variations in amplitude of the potential, as happens when $l_h \sim 10$ (significant deviations are observed for $l_h = 4$ and $l_h = 32$).

Finally, simulations have been performed to examine the role of the position of defects in the overall permeation. Figure 6 summarizes results from various configurations for two different heterogeneity (periodicity) scales as indicated. In panel a, various fractions of defects are introduced near the low-pressure side, whereas in panel b, they are introduced near the high-pressure side. Comparison between the two panels indicates an asymmetry in operation mode, due to the position of defects, as illustrated by differences of up to a factor of two in fluxes, for the same fraction of defects. In particular, it appears that defects are much more important in regions close to the inlet (high-pressure side), where the concentrations are high and interaction forces contribute largely to the local behavior. In high concentration regimes, the scale of the heterogeneity also plays an important role as seen in panel b.

Recent laser confocal optical microscopy studies of the microstructure of zeolite membranes (see also Figure 2f) indicate that membranes fabricated using the secondary growth technique, that is, formed from deposition of an initial coat-

ing of particles on a substrate, have larger grain boundaries near the zeolite/substrate interface (Bonilla et al., 2001). As a result, one may expect an asymmetry in fluxes in the case of strong intermolecular forces, depending on which side is exposed to the high-pressure stream.

Conclusions

A new mathematical framework linking molecular scale information with macroscopic scale (effective) properties of heterogeneous materials was introduced. Heterogeneity in materials is the rule rather than the exception in practice. The approach presented here was applied to the permeation of 2-D model membranes. The proposed approach replaces molecular (kinetic Monte Carlo) simulations with a mesoscopic approach that enables us to reach longer time and length scales. Furthermore, due to its continuum nature, mesoscopic models render the inclusion of heterogeneity over various scales tractable through the use of homogenization techniques. Direct numerical simulations were also carried out giving good agreement with the results obtained using homogenization. The influence of the nature of the heterogeneity (potential and diffusivity) and the effect of defect density and dispersion were also examined to qualitatively delineate the relationship between material structure and effective properties.

We have found that, as expected, the introduction of heterogeneity significantly affects the permeation properties. Furthermore, heterogeneity can also make evident uphill diffusion. Although, defect density plays a significant role in the permeation properties, defect dispersion is also important giving rise to asymmetric permeation behavior when intermolecular forces are significant. Finally, although physical conclusions were drawn, our focus has been on the proof of the concept, namely, the applicability of homogenization techniques, widely used for modeling of mechanical properties of composite materials, to systems with interparticle interactions. This framework offers a promising approach for modeling complex systems with heterogeneities, such as polycrystalline membranes, in which molecular scale information dictates macroscopic properties. Future work will focus on specific systems.

Acknowledgments

This research was partially supported by National Science Foundation through CTS-9702615, CTS-9904242, DMS-9626904, and DMS-9801769.

Literature Cited

Allen, M. P., and D. J. Tildesley, *Computer Simulation of Liquids*, Oxford Science Publications, Oxford (1989).

Auerbach, S. M., "Theory and Simulation of Jump Dynamics, Diffusion and Phase Equilibrium in Nanopores," *Int. Rev. Phys. Chem.*, **19**, 155 (2000).

Auriault, J.-L., and H. I. Ene, "Macroscopic Modelling of Heat Transfer in Composites with Interfacial Thermal Barrier," *Int. J. of Heat and Mass Transfer*, **37**, 2885 (1994).

Bensoussan, A., J.-L. Lions, and G. Papanicolaou, *Asymptotic Analysis for Periodic Structures*, North-Holland, Amsterdam, New York (1978).

Beylkin, G., "On the Fast Fourier Transform of Functions with Singularities," *Appl. Comput. Harmon.*, **2**, 363 (1995).

Binder, K., ed., *Monte Carlo Methods in Statistical Physics*, Springer-Verlag, Berlin (1986).

Binder, K., "Atomistic Modeling of Materials Properties by Monte-Carlo Simulation," *Adv. Mat.*, **4**, 540 (1992).

Bonilla, G., M. Tsapatsis, D. G. Vlachos, and G. Xomeritakis, "Fluorescence Confocal Optical Microscopy of the Grain Boundary Structure of Zeolite MFI Membranes made by Secondary (Seeded) Growth," *J. Memb. Sci.*, **182**, 103 (2001).

Bortz, A. B., M. H. Kalos, and J. L. Lebowitz, "A New Algorithm for Monte Carlo Simulations of Ising Spin Systems," *J. Comp. Phys.*, **17**, 10 (1975).

Bouddour, A., J.-L. Auriault, and M. Mhamdi-Alaqui, "Heat and Mass Transfer in Wet Porous Media in Presence of Evaporation-Condensation," *Int. J. of Heat and Mass Transfer*, **41**, 2263 (1998).

Chuan Kang, H., and W. H. Weinberg, "Modeling the Kinetics of Heterogeneous Catalysis," *Chem. Rev.*, 95, 667 (1995).

Cioranescu, D., and J. Saint Jean Paulin, *Homogenization of Reticulated Structures*, Springer-Verlag, New York (1998).

Cruz, M. E., and A. T. Patera, "A Parallel Monte-Carlo Finite-Element Procedure for the Analysis of Multicomponent Random Media," *Int. J. for Num. Methods in Eng.*, **38**, 1087 (1995).

Cummings, P. T., B. K. Peterson, C. K. Hall, M. Neurock, A. Z. Panagiotopoulos, and P. R. Westmoreland, "Future Directions in Molecular Modeling and Simulation: Fundamentals and Applications," *NSF Workshop Report*, available on the web at http://flory.engr.utk.edu/nsf (1997).

De Masi, A., E. Orlandi, E. Presutti and L. Triolo, "Stability of the Interface in a Model of Phase Separation," *Proc. Royal Soc. Edinb*, **124A**, 1013 (1994).

Giacomin, G., and J. L. Lebowitz, "Phase Segregation Dynamics in Particle Systems with Long Range Interactions: II. Interface Motion," *SIAM J. Appl. Math.*, **58**, 1707 (1998).

Gillespie, D. T., "A General Method for Numerically Simulating the Stochastic Evolution of Coupled Chemical Reactions," *J. Comp. Phys.*, **22**, 403 (1976).

Gillespie, D. T., "Exact Stochastic Simulation of Coupled Chemical Reactions," *J. Phys. Chem.*, **81**, 2340 (1977).

Gilmer, G., "Computer Models of Crystal Growth," *Science*, **208**, 355 (1980).

Gomer, R., "Diffusion of Adsorbates on Metal Surfaces," *Rep. Prog. Phys.*, **53**, 917 (1990).

Hildebrand, M., and A. S. Mikhailov, "Mesoscopic Modeling in the Kinetic Theory of Adsorbates," *J. Phys. Chem.*, **100**, 19089 (1996).

Hildebrand, M., A. S. Mikhailov and G. Ertl, "Nonequilibrium Stationary Microstructure in Surface Chemical Reactions," *Phys. Rev. E*, **58**, 5483 (1998).

Horntrop, D. J., M. A. Katsoulakis, and D. G. Vlachos, "Spectral Methods for Mesoscopic Models of Pattern Formation," *J. Comp. Phys.*, **173**, 364 (2001).

Katsoulakis, M. A., and D. G. Vlachos, "Mesoscopic Modeling of Surface Processes," *Multiscale Models for Surface Evolution and Reacting Flows*, C. Ringhofer, ed., Springer-Verlag, IMA, in press (2002).

Keil, F. J., R. Krishna, and M. O. Coppens, "Modeling of Diffusion in Zeolites," *Rev. Chem. Eng.*, **16**, 71 (2000).

Kelley, C. T., Iterative Methods for Linear and Nonlinear Equations: Matlab Codes (1995).

Lam, R., Atomistic-Continuum Hybrid Models for Epitaxial Growth of Materials and Homogenized Mesoscopic Theories for Diffusion through Nanoporous Films, MS Thesis, Dept. of Chemical Engineering, University of Massachusetts, Amherst (2001).

Lam, R., T. Basak, D. G. Vlachos, and M. A. Katsoulakis, "Validation of Mesoscopic Theories and Their Application to Computing Effective Diffusivities," *J. Chem. Phys.*, **115**, 11278 (2001).

Mei, C. C., J.-L. Auriault, and C.-O. Ng, "Some Applications of the Homogenization Theory," *Advances in Applied Mechanics*, Vol. 32, J. W. Hutchinson and T. Y. Wu., eds., Academic Press, San Diego, p. 277 (1996).

Metropolis, N., A. W. Rosenbluth, M. N. Rosenbluth, A. H. Teller, and E. Teller, "Equation of State Calculations by Fast Computing Machines," *J. Chem. Phys.*, **21**, 1087 (1953).

Murad, M. A., "Thermomechanical Model of Hydration Swelling in Smectitic Clays: I. Two-Scale Mixture-Theory Approach," *Int. J. for Numerical and Analytical Methods in Geomechanics*, **23**, 673 (1999).

Poutet, J., D. Manzoni, F. Hage-Chehade, C. J. Jacquin, M. J. Bouteca, J.-F. Thovert and P. M. Adler, "The Effective Mechanical Properties of Random Porous Media," *J. of Mechanics and Physics of Solids*, **44**, 1587 (1996).

Press, W. H., B. P. Flannery, S. A. Teukolsky and W. T. Vetterling, *Numerical Recipes*, Cambridge University Press, Cambridge (1986).

Reese, J., S. Raimondeau, and D. G. Vlachos, "Monte Carlo Algorithms for Complex Surface Reaction Mechanisms: Efficiency and Accuracy," *J. Comp. Phys.*, 173, 302 (2001).

Sanchez-Palencia, E., *Non-Homogeneous Media and Vibration Theory*, Springer-Verlag, Berlin and New York (1980).

Sanchez-Palencia, E. and A. Zaoui, *Homogenization Techniques for Composite Media: Lectures Delivered at the CISM International Center for Mechanical Sciences*, Udine, Italy, July 1–5, 1985, Springer-Verlag, Berlin and New York (1986).

Thompson, T. B., "Chemical Industry of the Future: Technology Roadmap for Computational Chemistry," *DOE Workshop Roadmap for Computational Chemistry*, available on the web at http://itri.loyola.edu/molmodel (1999).

Trefethen, L. N., *Spectral Methods in MATLAB*, Society for Industrial and Applied Mathematics (SIAM), Philadelphia, PA (2000).

Tsikoyiannis, J. G., and J. Wei, "Diffusion and Reaction in High-Occupancy Zeolite Catalysts: I. A Stochastic Theory," *Chem. Eng. Sci.*, **46**, 233 (1991).

Turing, A., "The Chemical Basis of Morphogenesis," *Phil. Trans. R. Soc. (London) Ser. B*, **237**, 37 (1952).

Vlachos, D. G., and M. A. Katsoulakis, "Derivation and Validation of Mesoscopic Theories for Diffusion of Interacting Molecules," *Phys. Rev. Lett.*, **85**, 3898 (2000).

Zhdanov, V. P., and B. Kasemo, "Kinetic Phase Transitions in Simple Reactions on Solid Surfaces," *Surf. Science Reports*, **20**, 111 (1994).

Ziff, R. M., E. Gulari and Y. Barshad, "Kinetic Phase Transitions in an Irreversible Surface-Reaction Model," *Phys. Rev. Lett.*, **56**, 2553 (1986).

Manuscript received July 3, 2001, and revision received Nov. 12, 2001.